

61

THE DENSITY MATRIX OF  $\text{H}_2\text{O} - \text{N}_2$  IN THE COORDINATE REPRESENTATION:  
A MONTE CARLO CALCULATION OF THE FAR-WING LINE SHAPE

Q. Ma

Department of Applied Physics, Columbia University  
and Institute for Space Studies, Goddard Space Flight Center  
2880 Broadway  
New York, New York 10025

and

R. H. Tipping

Department of Physics & Astronomy, University of Alabama  
Tuscaloosa, AL 35487-0324

*J. Chem. Phys.*

## ABSTRACT

The far-wing line shape theory within the binary collision and quasistatic framework has been developed using the coordinate representation. Within this formalism, the main computational task is the evaluation of multidimensional integrals whose variables are the orientational angles needed to specify the initial and final positions of the system during transition processes. Using standard methods, one is able to evaluate the 7-dimensional integrations required for linear molecular systems, or the 7-dimensional integrations for more complicated asymmetric-top (or symmetric-top) molecular systems whose interaction potential contains cyclic coordinates. In order to obviate this latter restriction on the form of the interaction potential, a Monte Carlo method is used to evaluate the 9-dimensional integrations required for systems consisting of one asymmetric-top (or symmetric-top) and one linear molecule, such as  $\text{H}_2\text{O} - \text{N}_2$ . Combined with techniques developed previously to deal with sophisticated potential models, one is able to implement realistic potentials for these systems and derive accurate, converged results for the far-wing line shapes and the corresponding absorption coefficients. Conversely, comparison of the far-wing absorption with experimental data can serve as a sensitive diagnostic tool in order to obtain detailed information on the short-range anisotropic dependence of interaction potentials.

## I. INTRODUCTION

In two recent papers,<sup>1,2</sup> we reported progress made to overcome the two main uncertainties remaining in the calculation of accurate far-wing line shapes. In the first paper,<sup>1</sup> we introduced the idea of formulating the theory using the coordinate representation instead of the state representation. The motivation resulted from efforts to calculate converged line shapes for complicated molecular systems. In previous calculations,<sup>3,4</sup> the states of the two interacting molecules were chosen as the complete set of basis functions in Hilbert space. These basis functions are characterized by well defined values of the energy, but not locations in space. As a result, one had to diagonalize anisotropic potential matrices because the latter are off-diagonal in this representation. However, it is well known that to diagonalize a matrix exhausts computer resources very quickly as the size of the matrix increases. Despite attempts to arrange the matrix in block-diagonal form which reduces the calculational cost significantly, the goal of obtaining converged results within reasonable computer CPU and memory constraints could only be achieved for the simplest systems such as  $\text{CO}_2 - \text{Ar}$ . By contrast, using the coordinate representation whose basis functions are characterized by the definite locations in space but not values of the energy, the diagonalization of the anisotropic potential matrix becomes unnecessary and the main computational task is transformed to the carrying out of multidimensional integrations over the continuous variables needed to specify the initial and final orientations of the two interacting molecules. For systems consisting of two linear molecules, or one linear and one more complicated (asymmetric-top or symmetric-top) molecule, or two complicated ones, the dimensionality of the integrations is seven, nine, and eleven, respectively. Then, as many states as desired can be included in the calculations and the convergence criterion is transformed to the feasibility of calculating these integrations within reasonable CPU time. In comparison with the previous requirement,<sup>3,4</sup> this new criterion is much less stringent. We applied this formalism for linear molecular systems ( $\text{CO}_2 - \text{CO}_2$  and  $\text{CO}_2 - \text{N}_2$ ) and showed that one

could evaluate the 7-dimensional integrations using standard methods and obtained converged results with modest CPU time.<sup>1</sup>

The other uncertainty is related to forms of the interaction potential that could be incorporated in the theory. It is well known that the theoretical line shape depends sensitively on the potential, especially on its short-range part. However, in previous formulations because of the necessity of finding roots of the radial part, the potential models that could be treated were limited to those having simple forms and one would not expect them to model the detailed interactions well. Therefore, an extension to more sophisticated potentials was necessary. In order to achieve this, we developed an interpolation procedure in which one does not have to find the roots directly; this advance enabled us to implement more realistic interaction potentials. The details of this technique were given in the second paper,<sup>2</sup> and combining this improvement with the coordinate representation, allowed us to calculate converged results for far-wing line shapes of linear molecular systems using realistic interaction potentials. More specifically, in a related paper,<sup>5</sup> we showed that using a sophisticated potential, one could calculate absorption coefficients that were in good agreement with experimental data over a range of temperatures for  $\text{CO}_2 - \text{CO}_2$ .<sup>5</sup>

However, if we extend our method to other complicated cases (e.g.,  $\text{H}_2\text{O} - \text{N}_2$  or  $\text{H}_2\text{O} - \text{H}_2\text{O}$ ), we found that the calculation of the higher-dimensional integrations is not feasible using standard methods. This implies that for these systems using standard methods, one has somehow to reduce the dimensionality of integrations required in numerical evaluations or to explore alternative methods to evaluate the higher-dimensional integrals.

In the second paper,<sup>2</sup> we presented progress made according to the first procedure. We found that for cases where the interaction potential considered contains cyclic coordinates, the integration over them can be carried out analytically, with the concomitant reduction of the dimensionality of the remaining numerical integrations. The

later can then be carried out using standard methods. Because the leading long-range anisotropic interaction contains such cyclic coordinates, one can adopt a short-range interaction having the same symmetry. In comparison with results computed with less sophisticated potentials for the same systems, the latter results are in better agreement with experiment.

In the present paper, we report results made by an alternative calculation of the multidimensional integrations using Monte Carlo methods. As a first step, we focus on systems containing one linear molecule. We show that by using the Monte Carlo technique, one can calculate the required 9-dimensional integrations and obtain converged results for the far-wing line shape using computational resources comparable to those needed to compute the 7-dimensional integrations using standard methods. Given the fact that we can consider potentials without cyclic coordinates, the advantages of the present method are obvious.

The organization of the present paper is as follows: In Sect. II we give a summary of the general formalism. Starting in Sect. II A, we outline the relation between the spectral density, the Fourier transform of the dipole moment autocorrelation function, and the band-averaged line shape. In Sect. II B, we discuss the density matrix expressed in the coordinate representation that is central to the calculation of the far-wing line shape; we derive explicit expressions applicable for an asymmetric-top molecule and calculate the density matrix of  $\text{H}_2\text{O}$  for several different temperatures. We present representative two-dimensional plots in order to illustrate the main contour features. In Sect. II C, we discuss in detail the interaction potential used in the present calculation without the restriction of cyclic coordinates. This consists of the long-range dipole-quadrupole interaction varying as  $r^{-4}$ , where  $r$  is the separation between centers of mass of the interacting molecules, an attractive dispersion term varying as  $r^{-6}$  containing an adjustable strength, and a short-range exponential site-site repulsive interaction containing four adjustable parameters. In Sect. II D, we discuss the Monte Carlo calculation of the

9-dimensional integrations and the results obtained. In the final Sect., we present a brief discussion of these results and the conclusions drawn from the present study, including reasons why previous interaction potentials utilized for the calculation of the Lorentzian half-widths<sup>6,7</sup> are not suitable for the far-wing calculation. In fact, the accurate representation of the far-wing line shape places severe restrictions on the short-range interaction and can be used to discriminate between various potential models giving comparable results for other calculated quantities.

## II. THE GENERAL FORMALISM

### A. The spectral density and the band-average line shape function

As shown in a previous study,<sup>4</sup> based on the binary collision approximation valid in the low-density limit, one is able to derive an expression for the spectral density  $F(\omega)$  as a summation of contributions from individual lines with the common line shape (i.e., the band-average line shape) denoted by  $\hat{\chi}(\omega)$ :

$$F(\omega) = \frac{1}{\pi} \sum_{\omega_{ij} > 0} e^{-\hbar(\omega - \omega_{ij})/2kT} \left\{ \frac{1}{(\omega - \omega_{ij})^2} \hat{\chi}(\omega - \omega_{ij}) + \frac{1}{(\omega + \omega_{ij})^2} \hat{\chi}(\omega + \omega_{ij}) \right\} \rho_i |\mu_{ij}|^2, \quad (1)$$

where the indices  $i$  or  $j$  represent all the quantum numbers necessary to specify the energy levels of the absorber molecule,  $\omega_{ij}$  are the resonance frequencies,  $\rho_i$  are the diagonal elements of the density matrix, and  $\mu_{ij}$  are the reduced dipole matrix elements. Within the quasistatic approximation valid for the far-wing line shape, one can calculate the band-average line shape  $\hat{\chi}(\omega)$  from knowledge of the interaction between two molecules. By choosing the  $Z$  axis of the space-fixed frame along the separation between the two molecules, the interaction  $V(\mathbf{r}, \Omega_a, \Omega_b)$  depends on the orientations of the molecules represented by  $\Omega_a$  and  $\Omega_b$ , respectively, and on  $\mathbf{r}$ . Within the quasistatic approximation, the translational motion is treated classically while the internal degrees of freedom are treated quantum mechanically. In Hilbert space associated with the internal degrees, one

denotes the eigenvalues and eigenvectors of  $V(\mathbf{r}, \Omega_a, \Omega_b)$  by  $G_\zeta$  and  $|\zeta\rangle$ , respectively; thus

$$V(\mathbf{r}, \Omega_a, \Omega_b)|\zeta\rangle = G_\zeta(\mathbf{r})|\zeta\rangle, \quad (2)$$

where  $\mathbf{r}$  appears in the eigenvalues  $G_\zeta(\mathbf{r})$  as a parameter. Then, one is able to derive an explicit expression for the band-average line shape  $\hat{\chi}(\omega)$ :

$$\hat{\chi}(\omega) = 4\pi^2 n_b \omega^2 \sum |\langle \zeta | \sqrt{\rho_a \rho_b} \mu | \eta \rangle|^2 \times r_c^2 \left| \frac{1}{G_{\zeta\eta}^i(r_c)} \right| e^{-[G_{\zeta\eta}^i(r_c) + G_\eta(r_c)]/2kT - V_{iso}(r_c)/kT} / \sum_{ij} \rho_i |\mu_{ij}|^2, \quad (3)$$

where  $n_b$  is the number density of the bath molecules,  $G_{\zeta\eta}^i(r)$  denotes  $\frac{d}{dr}[G_\zeta(r) - G_\eta(r)]$ , and  $r_c$  are roots of the equation

$$G_\zeta(r_c) - G_\eta(r_c) = \omega. \quad (4)$$

In order to carry out numerical calculations of  $\hat{\chi}(\omega)$  from Eq. (4), one first has to find the eigenvectors and eigenvalues of the potential and then sum the contributions resulting from all possible combinations of these eigenvectors representing the initial and final positions of the system during the transition processes. It has been shown that if the states of the system are chosen as the complete set of basis functions in Hilbert space, one is unable to obtain converged results except for the simplest systems such as  $\text{CO}_2 - \text{Ar}$  because a diagonalization procedure required exhausts computer resources quickly. In order to overcome this difficulty, a new method was developed recently in which the eigenfunctions of the orientations of the system are chosen as the complete set in Hilbert space.<sup>1</sup> From the theoretical point of view, these two methods are equivalent since they differ only by the choice of representation, but in practical calculations, the latter has a big advantage over the former. In fact, with the new method the diagonalization procedure is unnecessary and the main computational task is transformed to the carrying out of multidimensional integrations over the continuous orientational variables. With this formulation, we have shown that using standard methods, one is able to calculate converged results for systems consisting of two linear molecules in which the dimensionality of the integrations is seven.<sup>1,5</sup> For systems involving more complicated molecules, such as

$\text{H}_2\text{O} - \text{N}_2$  and  $\text{H}_2\text{O} - \text{H}_2\text{O}$ , the dimensionality of the integrations becomes nine and eleven, respectively, since more angular variables are needed to specify their orientations. Usually, standard methods are not applicable in order to evaluate such high multidimensional integrations. Recently, we have shown that in cases where the interaction potentials contain cyclic coordinates, one can carry out the integrations of the density matrix over these coordinates analytically first and obtain the "averaged" density matrix.<sup>2</sup> Then, with the "averaged" density matrix, one is able to reduce the dimensionality of the remaining integrations for both  $\text{H}_2\text{O} - \text{N}_2$  and  $\text{H}_2\text{O} - \text{H}_2\text{O}$  to seven, the same as those for linear molecular systems. As a result, one can obtain converged results using the standard methods. Although the leading terms of the long-range interactions of  $\text{H}_2\text{O} - \text{N}_2$  and  $\text{H}_2\text{O} - \text{H}_2\text{O}$  do have such cyclic coordinates, to require the other parts, especially the short-range part which is not known well at present, to have the same symmetry is a simplifying assumption which one would like to avoid.

It has been known for a long time that Monte Carlo methods can be applied for evaluating high multidimensional integrations. Given the fact that a calculated line shape ranges from line center to more than  $1000 \text{ cm}^{-1}$  away and requires a lot of points to depict well, we note that the complexity associated with the line shape calculation is greater than the evaluation of a few 9- or 11-dimensional integrations. As a first attempt, without introducing any assumptions on the symmetry of the  $\text{H}_2\text{O} - \text{N}_2$  interaction, we use the Monte Carlo method to directly evaluate the 9-dimensional integrations and calculate the line shape. By doing so, instead of the "averaged" density matrix of  $\text{H}_2\text{O}$ , the complete density matrix has to be used.

## B. The density matrix in the coordinate representation

Within the band-average approximation, we have shown that one can replace  $|\langle \zeta | \sqrt{\rho_a \rho_b} \mu | \eta \rangle|^2$  by  $|\langle \zeta | \sqrt{\rho_a \rho_b} | \eta \rangle|^2$  in the expression for the band-average line shape.<sup>1</sup> In later derivations, formulas without the subscripts a or b attached are understood to be

applicable for both the absorber and bath molecules.

In the following derivations, we adopt the simplifying notation that  $\Omega_\zeta$  is used to represent the orientation of the molecule of interest. For  $N_2$ ,  $\Omega_\zeta$  corresponds to  $\theta_\zeta$  and  $\varphi_\zeta$ . Alternatively, for the asymmetric-top  $H_2O$  molecule, it corresponds to  $\alpha_\zeta$ ,  $\beta_\zeta$ , and  $\gamma_\zeta$ .

Then, expressing  $|\zeta\rangle$  as

$$|\zeta\rangle = |\delta(\Omega_a - \Omega_{a\zeta}) \delta(\Omega_b - \Omega_{b\zeta})\rangle, \quad (5)$$

one is able to write  $|\langle \zeta | \sqrt{\rho_a \rho_b} | \eta \rangle|^2$  as the product of two factors

$$\begin{aligned} |\langle \zeta | \sqrt{\rho_a \rho_b} | \eta \rangle|^2 &= |\langle \delta(\Omega_a - \Omega_{a\zeta}) | \sqrt{\rho_a} | \delta(\Omega_a - \Omega_{a\eta}) \rangle|^2 \\ &\quad \times |\langle \delta(\Omega_b - \Omega_{b\zeta}) | \sqrt{\rho_b} | \delta(\Omega_b - \Omega_{b\eta}) \rangle|^2. \end{aligned} \quad (6)$$

The explicit expression for each factor depends on which class the molecule of interest belongs to. For linear molecules, we have shown that<sup>1</sup>

$$|\langle \delta(\Omega - \Omega_\zeta) | \sqrt{\rho} | \delta(\Omega - \Omega_\eta) \rangle|^2 = \sum_L A_L P_L(\cos\Theta_{(\zeta\eta)}), \quad (7)$$

where  $P_L(\cos\Theta_{(\zeta\eta)})$  are Legendre polynomials with  $L = 0, 1, 2, \dots$ , and  $\Theta_{(\zeta\eta)}$  is the angle between  $\Omega_\zeta$  and  $\Omega_\eta$ , viz.

$$\cos\Theta_{(\zeta\eta)} = \cos\theta_\zeta \cos\theta_\eta + \sin\theta_\zeta \sin\theta_\eta \cos(\varphi_\zeta - \varphi_\eta). \quad (8)$$

The coefficients  $A_L$  are given by

$$A_L = \frac{1}{16\pi^2 Q} \sum_{jj'} (2j+1)(2j'+1) \sqrt{g_j g_{j'}} e^{-[E(j)+E(j')]/2kT} C^2(j j' L, 0 0 0), \quad (9)$$

where  $Q$  is the partition function,  $g_j$  is the nuclear spin degeneracy factor,  $E(j)$  are the energies of the state corresponding to the angular quantum number  $j$ , and  $C(j j' L, 0 0 0)$  is a Clebsch–Gordan coefficient. The absolute square of the density matrix for  $N_2$  calculated from Eqs. (7) and (9) at  $T = 296, 338, \text{ and } 430 \text{ K}$  with a cut-off  $j_{\max} = 80$  are shown in Fig. 1. As shown in the figure, there are two sharp and uneven peaks located around  $\Theta_{(\zeta\eta)} = 0$  and  $180$  degrees, respectively, and the magnitude decreases very fast as  $\Theta_{(\zeta\eta)}$  differs from these values. By comparing the profiles obtained from different temperatures, it is obvious that the higher the temperature, the higher and narrower the peaks become. The more detailed discussions were reported previously.<sup>1</sup>

For a symmetric-top molecule whose wavefunctions are given by<sup>8</sup>

$$|jkm\rangle = (-1)^{m-k} \left(\frac{2j+1}{8\pi^2}\right)^{\frac{1}{2}} D_{-m,-k}^j(\alpha, \beta, \gamma), \quad (10)$$

where  $D_{m,k}^j(\alpha, \beta, \gamma) (= e^{-im\alpha} d_{m,k}^j(\beta) e^{-ik\gamma})$  is the rotational matrix, we have shown<sup>2</sup> that

$$|\langle \delta(\Omega - \Omega_\zeta) | \sqrt{\rho} | \delta(\Omega - \Omega_\eta) \rangle|^2 = \sum_{LK} A_{LK} D_{K,K}^L(\alpha_{(\zeta\eta)}, \beta_{(\zeta\eta)}, \gamma_{(\zeta\eta)}). \quad (11)$$

In Eq. (11),  $\alpha_{(\zeta\eta)}$ ,  $\beta_{(\zeta\eta)}$ , and  $\gamma_{(\zeta\eta)}$  are the three Euler angles used to represent a rotation resulting from two successive rotations, i.e.,

$$R(\alpha_{(\zeta\eta)}, \beta_{(\zeta\eta)}, \gamma_{(\zeta\eta)}) = R^{-1}(\alpha_\zeta, \beta_\zeta, \gamma_\zeta) R(\alpha_\eta, \beta_\eta, \gamma_\eta), \quad (12)$$

the summation index  $L = 0, 1, 2, \dots$  and the index  $K = -L, -L+1, \dots, L-1, L$ , respectively, and the coefficients  $A_{LK}$  are given by

$$A_{LK} = \frac{1}{64\pi^4 Q} \sum_{jj'} \sum_k (2j+1)(2j'+1) \sqrt{g_k g_{k-K}} e^{-[E(j,k)+E(j',k-K)]/2k_b T} C^2(jj' L, k K-k K), \quad (13)$$

where  $E(j,k)$  are the energies of the state labeled by the quantum numbers  $j$  and  $k$ , and  $g_k$  is its nuclear spin degeneracy factor. We note that when the quantum number  $k$  and the Boltzman constant  $k$  appear in same expressions, a subscript  $b$  is attached to the latter.

Similar expressions can also be derived for the asymmetric-top molecule whose wavefunctions are given in terms of an expansion of symmetric-top wavefunctions,<sup>9</sup>

$$|j\tau m\rangle = \sum_k U_{k\tau}^j |jkm\rangle. \quad (14)$$

In this case, we have shown<sup>2</sup> that

$$|\langle \delta(\Omega - \Omega_\zeta) | \sqrt{\rho} | \delta(\Omega - \Omega_\eta) \rangle|^2 = \sum_L \sum_{KK'} A_{KK'}^L D_{K,K'}^L(\alpha_{(\zeta\eta)}, \beta_{(\zeta\eta)}, \gamma_{(\zeta\eta)}), \quad (15)$$

where  $\alpha_{(\zeta\eta)}$ ,  $\beta_{(\zeta\eta)}$ , and  $\gamma_{(\zeta\eta)}$  are defined by Eq. (12) and the summation index  $L = 0, 1, 2, \dots$ , and both indices  $K$  and  $K'$  run from  $-L$  to  $L$ . In the above expression, the coefficients  $A_{KK'}^L$  are given by

$$A_{KK'}^L = \frac{1}{64\pi^4 Q} \sum_{jj'} \sum_{\tau\tau'} (-1)^{K+K'} (2j+1)(2j'+1) \sqrt{g_\tau g_{\tau'}} e^{-[E(j,\tau)+E(j',\tau')]/2k_b T}$$

$$\times \sum_{kk'} (-1)^{k+k'} U_{k\tau}^j U_{k'\tau}^j U_{k'-K'}^{j'} U_{k-K}^{j'} C(j j' L, k K-k K) C(j j' L, k' K'-k' K'), \quad (16)$$

where  $E(j, \tau)$  are the energies of the state, and  $g_\tau$  is its nuclear spin degeneracy factor. By comparing Eqs. (7), (11), and (15), i.e., the expressions for the factors associated with the linear, the symmetric-top and asymmetric-top molecules, respectively, it is obvious that the more complex the molecule, the more complex the expression becomes. In addition, for the linear molecule, the absolute square of the density matrix represents a one-dimensional distribution over the angle  $\Theta_{(\zeta\eta)}$ . Meanwhile, for the symmetric-top and asymmetric-top molecules, it can be understood as a three-dimensional distribution over the Euler angles  $\alpha_{(\zeta\eta)}$ ,  $\beta_{(\zeta\eta)}$ , and  $\gamma_{(\zeta\eta)}$ . For later convenience, we use the simple notation  $F(\alpha, \beta, \gamma)$  to represent it. We note that the normalization requirement is given by

$$\int_0^{2\pi} \int_0^\pi \int_0^{2\pi} F(\alpha, \beta, \gamma) \sin\beta \, d\alpha \, d\beta \, d\gamma = \frac{1}{8\pi^2}. \quad (17)$$

It has been shown<sup>1,2</sup> that one can easily include as many states as desired in numerical calculations for the density matrix of the linear molecules  $\text{CO}_2$  and  $\text{N}_2$  and also for the "averaged" density matrix of  $\text{H}_2\text{O}$ . In the present study, we note that one can still include all the states available in the calculations with affordable CPU costs. Although in order to calculate the density matrix for complex molecules there are many more individual coefficients  $A_{LK}^L$  and  $A_{KK}^L$ , needed, and their expressions become more complicated as shown by Eqs. (13) and (16), respectively, the calculation of these coefficients is straightforward. In addition, one does not need to calculate all of them since some of them are identical and others are zero. For the  $\text{H}_2\text{O}$  molecule of interest in the present study, it turns out that due to the symmetry of  $U_{k\tau}^j$  all the coefficients  $A_{KK}^L$ , are zero unless their indices  $K$  and  $K'$  have the same evenness or oddness. In addition, for the non-zero coefficients the following symmetries are valid:

$$A_{KK'}^L = A_{K'K}^L = A_{-K-K'}^L. \quad (18)$$

As a result, if  $j_{\max}$  is the highest angular quantum number of the states included in the calculation, one only needs to calculate the coefficients  $A_{KK}^L$ , for  $L = 0, 1, 2, \dots, L_{\max}$  where

$L_{\max} = 2j_{\max}$ , for  $K = 0, 1, 2, \dots, L$ , and for  $K' = -K, -K + 2, \dots, K - 2, K$ . The number of distinct coefficients is equal to  $(L_{\max} + 1)[1 + L_{\max}(L_{\max} + 5)/6]$ . As an example, for the pure rotational band of  $H_2O$ , the highest angular quantum number of the initial states listed in the HITRAN 92 database<sup>10</sup> is 23. If one includes all these states, there are 18424 coefficients needed to be evaluated. In comparison with the calculation of the "averaged" density matrix in which there are only 47 ( $= 2j_{\max} + 1$ ) coefficients  $A_L$  needed, of course, this requires a lot of more computation requiring several dozen hours to complete using a workstation. But, fortunately, for a specified temperature it needs to be done only once.

When all these  $A_{KK}^L$ , are available, one can easily obtain the density matrix given in the coordinative representation since the the expression for the rotational matrix is known. The explicit expression for  $F(\alpha, \beta, \gamma)$  used in the numerical calculations is given by

$$F(\alpha, \beta, \gamma) = \sum_L \sum_K \sum_{K'} A_{KK}^L \epsilon_{KK'} \cos[(K + K')(\alpha + \gamma)/2] \cos[(K - K')(\alpha - \gamma)/2] d_{KK}^L(\beta), \quad (19)$$

where  $\epsilon_{KK'} = 1$  for  $K = K' = 0$ ;  $\epsilon_{KK'} = 2$  for  $|K'| = K$ ;  $\epsilon_{KK'} = 4$  for  $|K'| \neq K$ , and the ranges of the indices  $L, K$ , and  $K'$  are from 0 to  $L_{\max}$ , from 0 to  $L$ , and from  $-K, -K + 2, \dots, K - 2, K$ , respectively. We note that in this expression, the Euler angles  $\alpha$  and  $\gamma$  appear not by themselves, but in the combinations  $(\alpha + \gamma)/2$  and  $(\alpha - \gamma)/2$ . In addition,  $(\alpha + \gamma)/2$  is associated with  $K + K'$ , and  $(\alpha - \gamma)/2$  is associated with  $K - K'$ . More discussion about this point is given later.

It has been shown<sup>2</sup> that the profile of the "averaged" density matrix of  $H_2O$  which is a one-dimensional distribution to some extent looks like a  $\delta$  function. One expects that the profile of the density matrix of  $H_2O$  itself which is a three-dimensional distribution exhibits more detailed features. Of course, it is impossible to plot  $F(\alpha, \beta, \gamma)$  in one figure and one has to present it using a series of two-dimensional contours with one argument fixed.

With Eq. (19), we calculate several two-dimensional distributions  $F(\alpha, \beta_0, \gamma)$  over

the Euler angles  $\alpha$  and  $\gamma$  at  $T = 296$  K obtained with  $\beta_0 = 0, 20, 40,$  and  $60$  degrees, respectively, and present their corresponding contour plots in Fig. 2. From this figure, one can draw two conclusions. By comparing these plots, one can easily find that the magnitudes of the density matrix decrease very fast as  $\beta_0$  increases. This is fully expected since the profile of the "averaged" density matrix known from a previous study exhibits this behavior. In fact, by carrying out a two-dimensional integration of the density matrix over the Euler angles  $\alpha$  and  $\gamma$ , one expects to obtain a one-dimensional distribution of the density matrix over the remaining angle  $\beta$ . This results in exactly the "averaged" density matrix as easily shown by

$$\begin{aligned} \int_0^{2\pi} \int_0^{2\pi} F(\alpha, \beta, \gamma) d\alpha d\gamma &= 4\pi^2 \sum_L A_{00}^L D_{0,0}^L(0, \beta, 0) \\ &= \sum_L A_L P_L(\cos\beta). \end{aligned} \quad (20)$$

In deriving the last step of Eq. (20), the fact that  $4\pi^2 A_{00}^L = A_L$  has been used and the explicit expression for  $A_L$  was given in our previous study.<sup>2</sup> Secondly, by analyzing each of these contours, it is obvious that these  $F(\alpha, \beta_0, \gamma)$  exhibit symmetry with respect to the axes  $(\alpha + \gamma)/2$  and  $(\alpha - \gamma)/2$ . It is interesting to note that if one introduces the two arguments  $u \equiv (\alpha + \gamma)/2$  and  $v \equiv (\alpha - \gamma)/2$ , the magnitudes of  $F(\alpha, \beta_0, \gamma)$  depend very sensitively on the former, but are insensitive to the latter, especially for the cases where  $\beta_0$  is small. This implies that instead of  $\alpha$  and  $\gamma$ , it is better to choose  $u$  and  $v$  as the two arguments. The same conclusion is also suggested by Eq. (19) as mentioned above. We use the symbol  $G(\beta, u, v)$  to represent the distribution of the density matrix over  $\beta, u,$  and  $v$ . We note that the values of  $u$  and  $v$  vary in a lozenge-shaped area, the former's maximum and minimum equal to  $0$  and  $2\pi$ , respectively, and the latter's are  $-\pi$  and  $\pi$ , respectively.

Since  $G(\beta, u, v)$  has one insensitive argument  $v$ , its profile can be well represented by one contour plot of  $\bar{G}(\beta, u)$  resulting from averaging over  $v$ . Due to the symmetry  $\bar{G}(\beta,$

$2\pi - u) = \overline{G}(\beta, u)$ , one can calculate values of  $\overline{G}(\beta, u)$  only in the range of  $v$  from 0 to  $\pi$ .

In this case,  $\overline{G}(\beta, u)$  is defined by

$$\overline{G}(\beta, u) = \frac{1}{2u} \int_{-u}^u G(\beta, u, v) dv. \quad (21)$$

With Eq. (19), one is able to carry out the above integration analytically and derive an explicit expression for  $\overline{G}(\beta, u)$  but this is not presented here. We calculated  $\overline{G}(\beta, u)$  for  $T = 296$  K, 338 K, and 430 K and present the results obtained in Figs. 3 – 5, respectively. In order to visualize the complete profiles of the density matrix, one can imagine that except for small deviations which can be ignored in small  $\beta$  areas, the profiles shown in Figs. 3 – 5 extend along another dimension, i.e., the  $v$  axis which is perpendicular to the  $\beta - u$  plane and is missing in these figures. Furthermore, the range of the extension along the  $v$  axis is equal to  $[-u, u]$ , which varies from the minimum 0 at  $u = 0$  to the maximum  $2\pi$  at  $u = \pi$ . From these figures, it is obvious that the density matrix of  $H_2O$  exhibits more structures than that shown by the "averaged" density matrix. Along the  $u$  axis, there are 5 sharp peaks located at  $(0, 0)$ ,  $(0, \pi/2)$ ,  $(0, \pi)$ ,  $(0, 3\pi/2)$  and  $(0, 2\pi)$ , respectively. The largest is the one at  $(0, \pi)$ . This conclusion results not only from its apparent size in the plots, but also from the fact that it extends along the  $v$  axis more than the others. With respect to its distributions along the  $\beta$  axis, in general, the density matrix of  $H_2O$  decreases very fast as  $\beta$  increases which has been shown previously for the "averaged" density matrix. On the other hand, by comparing the results obtained from different temperatures, one concludes that as the temperature increases, the peaks become sharper, i.e., their heights are higher and their widths are narrower. We note that in the contour plot obtained at  $T = 430$  K, the lowest scale is reduced from  $1.0 \times 10^{-13}$  used for  $T = 296$  K and 338 K to  $1.0 \times 10^{-10}$ . Otherwise, calculation errors add some meaningless structures in areas where the magnitudes are below this limit; this indicates a general trend that for higher temperatures more states with higher  $j$  values have to be added in the calculations.

In order to carry out line shape calculations, one can calculate  $G(\beta, u, v)$  and store

the results in files. The areas with high  $\beta$  values can be excluded from consideration. One can further reduce the ranges of  $u$  and  $v$  due to symmetry considerations. One has to choose high resolutions for  $\beta$  and  $u$ , but a lower one for  $v$ . The details are not presented here for brevity.

### C. More general potential models

In our previous study<sup>2</sup>, we have developed techniques to deal with complicated interaction potential models, specifically those for which their dependence on  $r$  and on  $\Omega_a$  and  $\Omega_b$  interweave, and the dependence on  $r$  takes a complicated form. For example, we can adopt a flexible site–site model,

$$V_{sr}(r, \Omega_a, \Omega_b) = \sum_{i \in a} \sum_{j \in b} V_{ij}(r_{ij}), \quad (22)$$

in modeling the short–range part of the anisotropic interaction. In this site–site model, the indices  $i$  and  $j$  run over force centers of the absorber molecule  $a$  and the perturber  $b$ , respectively,  $r_{ij}$  is the distance between the center  $i$  and the center  $j$ , and  $V_{ij}(r_{ij})$  represent individual interactions between them. The flexibility of the site–site model can be achieved by choosing different numbers of the centers, different locations of the centers, and different forms for  $V_{ij}$ . With respect to the long–range part of the anisotropic interaction, one usually adopts the leading term of the multipole expansion which, in the present case, is the dipole–quadrupole interaction given by

$$V_{dq}(r, \Omega_a, \Omega_b) = \frac{3\mu Q}{2r^4} [\cos\beta_a (3 \cos^2\theta_b - 1) - 2 \sin\beta_a \sin\theta_b \cos\theta_b \cos(\alpha_a - \varphi_b)], \quad (23)$$

where  $\mu$  is the dipole moment of  $H_2O$  lying along the  $Z$  axis of the body–fixed frame, and  $Q$  is the quadrupole moment of  $N_2$ .

It has been shown that in order to make multidimensional integrations tractable with standard methods, we had to limit potential models to those containing cyclic coordinates. The dipole–quadrupole interaction of  $H_2O - N_2$  has a cyclic coordinate  $\gamma_a$ . By assuming that in the site–site model the force centers of  $H_2O$  are located along the  $Z$

axis of the body-fixed frame,  $V_{sr}(r, \Omega_a, \Omega_b)$  has the same symmetry as  $V_{dq}(r, \Omega_a, \Omega_b)$ . With this restriction, one can introduce the "averaged" density matrix and reduce the original 9-dimensional integrations to 7-dimensional ones. Then, standard methods become applicable to carry out the integrations.

Since at present one does not know the short-range anisotropic interaction of  $H_2O - N_2$  well, it is desirable to consider more general models. Therefore, we adopt a site-site model having three force centers for  $H_2O$ : two located at the two H atoms and one at the O atom. With respect to the  $N_2$  molecule, we assume that there are two force centers and they are located on the two N atoms, the same as we did previously. Concerning the form of  $V_{ij}(r_{ij})$ , we assume that  $V_{ij}(r_{ij}) = A_{ij} e^{-r_{ij}/\rho_{ij}}$  to represent the repulsive interaction between force centers where  $A_{ij}$  and  $\rho_{ij}$  are adjustable parameters. In order to take into account attractive dispersion interaction, we include an isotropic term given by  $-B/r^6$  where B is an adjustable parameter. As a result, the potential  $V(r, \Omega_a, \Omega_b)$  considered is given by

$$V(r, \Omega_a, \Omega_b) = \sum_{i \in a} \sum_{j \in b} A_{ij} e^{-r_{ij}/\rho_{ij}} + V_{dq}(r, \Omega_a, \Omega_b) - \frac{B}{r^6}, \quad (24)$$

and it contains 5 adjustable parameters:  $A_{HN}$ ,  $\rho_{HN}$ ,  $A_{ON}$ ,  $\rho_{ON}$  and B. The dipole moment of  $H_2O$  and the quadrupole moment of  $N_2$  are well known and the values used in the present calculations are 1.8546 D and 1.40 D Å, respectively. Meanwhile, the bond angle of  $H_2O$  is 104.52 degrees and the separation between the O atom and the H atom is 0.9572 Å;<sup>11</sup> the separation of two N atoms of the  $N_2$  molecule is 1.10 Å.<sup>12</sup> By making these choices,  $V(r, \Omega_a, \Omega_b)$  depends on all 5 angular variables used to specify the orientations of  $H_2O - N_2$ . This implies that  $V(r, \Omega_a, \Omega_b)$  does not contain any cyclic coordinates and it is necessary to evaluate the 9-dimensional integration.

#### D. A Monte Carlo calculation of the line shapes

By choosing the eigenfunctions of the orientations of  $H_2O - N_2$  as the complete set

of basis functions, the summation over  $\zeta$  and  $\eta$  in Eq. (3) becomes 9-dimensional integrations over  $\beta_{a\zeta}$ ,  $\gamma_{a\zeta}$ ,  $\theta_{b\zeta}$ ,  $\varphi_{b\zeta}$ ,  $\alpha_{a\eta}$ ,  $\beta_{a\eta}$ ,  $\gamma_{a\eta}$ ,  $\theta_{b\eta}$ , and  $\varphi_{b\eta}$  in which the first four (including  $\alpha_{a\zeta} = 0$ ) specify the initial orientations of  $\text{H}_2\text{O} - \text{N}_2$  and the last five specify the final ones. We note that due to the rotational symmetry of the whole system, one can always assume  $\alpha_{a\zeta} = 0$ .

It has been known for years that the Monte Carlo method is an alternative way to calculate multidimensional integrations, especially in cases where their dimensionalities are so high that standard methods do not yield reliable results. We rely on an algorithm called VEGAS which is widely used in elementary particle physics.<sup>13</sup> As a Monte Carlo algorithm, VEGAS is primarily based on important sampling, but also does some stratified sampling. The important sampling is crucial in the present calculations since the distributions of the integrand over its 9 integration variables are extremely nonuniform. In fact, as shown by Eq. (3) it contains the factor  $|\langle \zeta | \sqrt{\rho_a \rho_b} \mu | \eta \rangle|^2$  which is the product of the density matrix of  $\text{H}_2\text{O}$  and the density matrix of  $\text{N}_2$ . As shown by Figs. 1 – 5, these density matrices are highly concentrated in narrow areas. As a result, one must use the important sampling to achieve variance reduction in Monte Carlo computations. This can easily be done by setting input flags in VEGAS. With VEGAS, the subroutine vegas performs  $m$  (the flag 1) statistically independent evaluations of the desired integral, each with  $N$  (the flag 2) integrand evaluations. While statistically independent, these iterations do assist each other, since each one is used to refine the sampling grid for the next one. The results of all integrations are combined into a single best answer and its estimated error. Interested readers can find its basic features in the book of Numerical Recipes in Fortran 77.<sup>13</sup>

We have made some modifications necessary in VEGAS resulting from special requirements in the line shape calculation. As mentioned previously, the complexity associated with the line shape calculations is far beyond the need to evaluate a few values of the 9-dimensional integrations. In practice, since the line shape is a function of

frequency, one has to use a lot of points to depict it well. Therefore, the number of the 9-dimensional integrations to be evaluated simultaneously by the algorithm is around 100 or so.

In order to verify the applicability of Monte Carlo algorithm in the line shape calculation, we have made several tests in which the potentials considered contain cyclic coordinates and 9-dimensional integrations can be reduced to 7-dimensional ones. In these cases, we use two methods to calculate the line shapes. First, by introducing the "averaged" density matrix and using standard methods, we carried out the reduced 7-dimensional integrations and obtained converged results. On the other hand, we used the Monte Carlo algorithm directly to evaluate 9-dimensional integrations. It turns out that in general, by taking around  $10^6$  or  $10^7$  random selections of a set of the 9 orientational variables, the Monte Carlo algorithm can produce line shapes without significant differences from those obtained before.<sup>2</sup> The CPU times required are modest on a workstation.

Then we applied the Monte Carlo method to cases where the potentials do not contain any cyclic coordinates. In order to verify the applicability, one can compare results obtained from the Monte Carlo algorithm with different random selection numbers and check whether results have converged. We present in Fig. 6 two line shapes obtained at  $T = 296$  K with the same potential parameters but with different numbers of the random selections. The first one is obtained from  $3.2 \times 10^6$  random evaluations of the integrand, i.e., a call of VEGAS with  $m = 3$  and  $N = 4 \times 10^5$  immediately followed by another call with  $m = 1$  and  $N = 2 \times 10^6$ . The second is from  $9.2 \times 10^6$  random evaluations using a call of VEGAS with  $m = 3$  and  $N = 4 \times 10^5$  immediately followed by another call with  $m = 1$  and  $N = 8 \times 10^6$ . From Fig. 6, it is obvious that there are only negligible differences between these two line shapes. Therefore, one can conclude that using approximately  $10^7$  random selections of the set of variables, the calculated line shapes are converged. It is interesting to note that the same number of terms is required to evaluate 7-dimensional

integrations using standard methods. This implies that with comparable computer resources (several hours CPU time at a workstation) required previously for 7-dimensional integrations, the Monte Carl algorithm enables us to evaluate 9-dimensional ones.

After making convergence tests, we know how many random evaluations are needed in order to obtain reliable results. Thus the only difficulty left in the line shape calculations, and consequently in the absorption coefficient calculations, is the choice of a realistic potential model. We adopt the potential form given by (24) and begin to search a set of potential parameters that enables us to get a good fit to the experimental results of Burch et al.<sup>14</sup> at  $T = 296$  K. We find that by adopting  $A_{\text{HN}}/k = 1.2 \times 10^6$  K,  $\rho_{\text{HN}} = 0.28$  Å,  $A_{\text{ON}}/k = 1.5 \times 10^8$  K,  $\rho_{\text{ON}} = 0.26$  Å, and  $B/k = 1.38 \times 10^6$  K, one is able to obtain satisfactory results. In addition, we note that because the short-range model has an isotropic contribution, which when combined with the isotropic dispersion interaction  $-B/r^6$ , gives "effective" Lennard-Jones parameters of  $\sigma_{\text{eff}} = 3.57$  Å, and  $\epsilon_{\text{eff}}/k = 207$  K, in reasonable agreement with other estimates. Based on this potential model, we calculated the the band-averaged line shapes of  $\text{H}_2\text{O} - \text{N}_2$  for several temperatures  $T = 296$  K, 338 K, and 430 K. The line shapes at  $T = 296$  K plotted in Fig. 6 are from these calculated results. The line shapes at  $T = 338$  K and 430 K, together with that at  $T = 296$  K, obtained from a call of VEGAS with  $m = 3$  and  $N = 4 \times 10^5$  immediately followed by another call with  $m = 1$  and  $N = 4 \times 10^6$ , are presented in Fig. 7. The  $\text{N}_2$ -broadened absorption coefficients at  $T = 296$  K in the spectral region  $300 - 1100$   $\text{cm}^{-1}$  based on HITRAN 92 data are plotted in Fig. 8, together with the experimental results of Burch et al.<sup>14</sup> Similarly, the calculated absorption at  $T = 430$  K and comparison with experimental data<sup>14</sup> are presented in Fig. 9. As shown by these figures, the agreement with the laboratory values is reasonably good.

### III. DISCUSSIONS AND CONCLUSIONS

In summary, there are three main theoretical improvements made recently in line

shape calculations. The first is that instead of the representation constructed from the states of the system, one uses the coordinate representation enabling one to avoid convergence errors resulting from the truncation of states included in calculations, and the failure to maintain the commutativity of the dipole moment and the anisotropic potential. We note that in practical calculations, the ability to overcome the convergence problem is crucial for the accurate calculation of the corresponding far-wing line shape.

The second improvement is the interpolation procedure introduced which obviates the need to find the roots in Eq. (4) and enables one to handle complicated potential forms. Given the fact that the calculated far-wing line shapes depend sensitively on the potential, especially on its short-range anisotropic part, and that the latter can not be represented well by simple models consisting of the Lennard-Jones isotropic potential and the leading term of the multipole expansion, the ability to incorporate more sophisticated potential models is crucial for realistic calculations. For linear molecular systems, it has been shown that the main computational task is to carry out 7-dimensional integrations and the later can be evaluated using standard methods. However, for systems involving complicated molecules, the generality of potential models is limited to those having cyclic coordinates. This restriction permits one to introduce the "averaged" density matrix in order to reduce the dimensionality of integrations to be evaluated. Otherwise, standard methods are not applicable for carrying out the required 9- or 11-dimensional integrations.

Finally, the Monte Carlo algorithm has been tested for line shape calculations. Based on numerical tests, one concludes that this method can be used, at least to evaluate 9-dimensional integrations. As a result, one can utilize sophisticated potential models for systems consisting of one asymmetric-top (or symmetric-top) molecule and one linear molecule and obtain converged results for the far-wing line shapes and corresponding absorption coefficients.

It has been shown in our previous study<sup>2</sup> that the far-wing shape is very sensitive to the angular gradients of the potential and, more specifically, to the detailed energy contour

area at which large angular gradients of the potential are exhibited while the potential values are relatively small or even negative. We expect that such features would not fully manifest their effects on other physical measurements (e.g., the second virial coefficient, the Lorentzian halfwidth and shift, etc.). This implies that the far-wing line shape can serve as a sensitive diagnostic tool to obtain detailed and desirable information about the interaction between two molecules. Given the fact that we can treat all potential models for  $\text{H}_2\text{O} - \text{N}_2$  and we have full confidence that the results obtained are the "true" values corresponding to these models, this role becomes even more valuable.

In the present work, we have tested some other models, such as a site-site model whose expression is given by

$$V(r, \Omega_a, \Omega_b) = \sum_{i \in a} \sum_{j \in b} 4\epsilon_{ij} \left[ \left( \frac{\sigma_{ij}}{r_{ij}} \right)^{12} - \left( \frac{\sigma_{ij}}{r_{ij}} \right)^6 \right], \quad (25)$$

where the individual interactions between force centers take the Lennard-Jones form and  $\epsilon_{ij}$  and  $\sigma_{ij}$  are corresponding parameters. It turns out that with the same parameters used in Lorentzian halfwidth and shift calculations,<sup>6,7</sup> the magnitudes of the calculated far-wing line shape are too large and predict much more absorption when compared with the measurements. By analyzing contour profiles of this model in detail, we find that its angular gradients are very large at some areas where the potential values are relatively small. This results from the Lennard-Jones form. It is well known that around  $r = \sigma$ , the value of the Lennard-Jones potential is close to zero, but its gradient in  $r$  is large. For each components  $V_{ij}$ , the same feature appears around  $r_{ij} = \sigma_{ij}$ . On the other hand, although the distance  $r$  between two molecules is assumed to be fixed during the transition process, all the distances between force center  $i$  and center  $j$ , i.e.,  $r_{ij}$  vary as the two molecules change their orientations. It happens that for some special positions of the system, one or more of these  $r_{ij}$  are close to  $\sigma_{ij}$ . Then, small rotations of the orientations could result in significant changes in the values of  $V_{ij}$ . As a result,  $V(r, \Omega_a, \Omega_b)$  could possess very large angular gradients and relatively small values near these special areas.

As mentioned above, most of significant contributions to the magnitudes of the far-wing line shape come from positions of the system such that around their energy contour area, large angular gradients of the potential are exhibited while the potential values are relatively small or even negative. The latter requirement can be easily understood since the system would have few statistical chances to occupy positions having large positive potential values. Therefore, it is not surprising that the potential model constructed from the Lennard-Jones form produces too large magnitudes of the far-wing line shape. The failure to predict the absorption indicates that the actual interaction is not well represented by this model. However, we note that this does not devalue its applicability for predicting different physical quantities which are insensitive to these features, but sensitive to other ones. The profile of the interaction potential between two molecules has a complicated nature which cannot be ascertained from only a single physical measurement; one has to combine all diagnostic means available to map its complexity.

Although the work performed in the present paper is for  $\text{H}_2\text{O} - \text{N}_2$ , similar studies can be carried out for other systems, such as  $\text{H}_2\text{O} - \text{CO}_2$ . However, one challenge still remains, i.e., how to deal with the  $\text{H}_2\text{O} - \text{H}_2\text{O}$  system for which one needs to evaluate 11-dimensional integrations if the potential considered does not contain any cyclic coordinates.

In general, to extend the Monte Carlo computations to higher dimensions may be possible. It will require more random selections to achieve converged results, but not 100 times more (a typical amount obtained by selecting 10 points along each additional dimension) as standard methods do. However, there is another difficulty faced by the Monte Carlo computations resulting from the integrand itself, i.e., that its distributions become even more nonuniform. In fact, the factor  $|\langle \zeta | \sqrt{\rho_a \rho_b} \mu | \eta \rangle|^2$  for  $\text{H}_2\text{O} - \text{H}_2\text{O}$  distributes nonuniformly over 6 variables in comparison with the  $\text{H}_2\text{O} - \text{N}_2$  case where it distributes nonuniformly only over 4 variables.

In addition, it has been shown in our previous studies<sup>1,2</sup> that it is essential to

separate the sensitive variables of the integrand from insensitive ones since this separation enables one to choose different resolutions in evaluating multidimensional integrations using standard methods. The same conclusion is also true in the Monte Carlo computations. In this case, the separation enables one to tailor the important sampling and to reduce the variance dramatically. This separation is achieved by representing the final orientations of the system labeled by  $\eta$  in terms of the body-fixed frames instead of the space-fixed frame. The body-fixed frames introduced here are those attached to the two molecules at their initial orientational positions. More explicitly, for the linear molecule, one chooses  $\theta_\zeta$ ,  $\varphi_\zeta$ ,  $\theta_{(\zeta\eta)}$ , and  $\varphi_{(\zeta\eta)}$  instead of  $\theta_\zeta$ ,  $\varphi_\zeta$ ,  $\theta_\eta$ , and  $\varphi_\eta$ ; for the symmetric-top or asymmetric-top molecule, one chooses  $\alpha_\zeta$ ,  $\beta_\zeta$ ,  $\gamma_\zeta$ ,  $\alpha_{(\zeta\eta)}$ ,  $\beta_{(\zeta\eta)}$ , and  $\gamma_{(\zeta\eta)}$  instead of  $\alpha_\zeta$ ,  $\beta_\zeta$ ,  $\gamma_\zeta$ ,  $\alpha_\eta$ ,  $\beta_\eta$ , and  $\gamma_\eta$ . However, it is necessary to carry out some algebra when one calculates potential values with these variables since the expressions for potentials are always given in terms of the space-fixed frame; thus, one has to rotate the body-fixed frame back to the space fixed one. The more complex the molecule, the more work is required.

Based on the arguments given above, it is obvious that more random selections and more CPU time will be required to achieve converged line shapes for  $\text{H}_2\text{O} - \text{H}_2\text{O}$ . However, without numerical tests, it is difficult to assert whether the Monte Carlo method is applicable for this system. We plan to pursue this problem in further research.

#### ACKNOWLEDGEMENT:

This work was supported in part by the Department of Energy Interagency Agreement under the Atmospheric Radiation Measurement Program, by NASA through grants NAG5-6314, NAG5-8269, and NAGW-4693. The authors would like to thank the National Energy Research Supercomputer (Livermore, CA) for computer time and facilities provided.

## LIST OF FIGURES

- Fig. 1. The absolute square of the density matrix of  $N_2$  given in the coordinate representation calculated at three temperatures for  $j_{\max} = 80$ : the solid line at  $T = 296$  K; the dashed - dotted line at  $T = 338$  K; and the dotted line at  $T = 430$  K.
- Fig. 2. The two-dimensional distributions of the density matrix of  $H_2O$  over the Euler angles  $\alpha$  and  $\gamma$  obtained at  $T = 296$  K for  $j_{\max} = 23$ . The value of the Euler angle  $\beta$  is fixed and there are four plots presented here corresponding to  $\beta = 0, 20, 40,$  and  $60$  degrees, respectively.
- Fig. 3. The two-dimensional distribution of the density matrix of  $H_2O$  over the two sensitive angles  $\beta$  and  $u [\equiv (\alpha + \gamma)/2]$  obtained at  $T = 296$  K for  $j_{\max} = 23$ . This distribution results from averaging the density matrix of  $H_2O$  over the one insensitive angle  $v [\equiv (\alpha - \gamma)/2]$ . The range of  $u$  is  $[0, 2\pi]$  and there is a symmetry respect to the axis  $u = \pi$ . The plot presented here covers  $0 \leq u \leq \pi$  only.
- Fig. 4. The same as Figure 3, except  $T = 338$  K.
- Fig. 5. The same as Figure 3, except  $T = 430$  K. In comparison with that used in Figures 3 and 4, the lowest scale is reduced to avoid meaningless structures which result from numerical errors. This indicates a general trend that for higher temperatures more states with higher  $J$  values have to be added in the calculations.
- Fig. 6. The  $N_2$ -broadened far-wing line shape of  $H_2O$  (in units of  $\text{cm}^{-1} \text{atm}^{-1}$ ) as a function of frequency  $\omega$  (in units of  $\text{cm}^{-1}$ ) for  $T = 296$  K calculated with two different numbers of random selections in the Monte Carlo calculation; they are obtained from  $9.2 \times 10^6$  and  $3.2 \times 10^6$  random evaluations of the integrand and are represented by the solid and dashed curves, respectively.
- Fig. 7. The  $N_2$ -broadened far-wing line shape of  $H_2O$  (in units of  $\text{cm}^{-1} \text{atm}^{-1}$ ) as a function of frequency  $\omega$  (in units of  $\text{cm}^{-1}$ ) for  $T = 296$  K,  $338$  K, and  $430$  K; these are represented by the solid, dashed, and dotted lines, respectively.
- Fig. 8. The calculated  $N_2$ -broadened absorption coefficient (in units of  $\text{cm}^2 \text{molecule}^{-1}$

atm<sup>-1</sup>) at  $T = 296$  K in the  $300 - 1100$  cm<sup>-1</sup> spectral region is represented by  $\Delta$ . For comparison, the experimental values are denoted by  $+$ .

Fig. 9. The same as Fig. 8, except that  $T = 430$  K.

## REFERENCES

- 1) Q. Ma and R. H. Tipping, *J. Chem. Phys.* **108**, 3386 (1998)
- 2) Q. Ma and R. H. Tipping, *J. Chem. Phys.*, **111**, in press (1999)
- 3) P. W. Rosenkranz, *J. Chem. Phys.* **83**, 6139 (1985); *J. Chem. Phys.* **87**, 163 (1987).
- 4) Q. Ma and R. H. Tipping, *J. Chem. Phys.* **95**, 6290 (1991); *J. Chem. Phys.* **96**, 8655 (1992); *J. Chem. Phys.* **97**, 818 (1992).
- 5) Q. Ma, R. H. Tipping, C. Boulet, and J. -P. Bouanich, *Appl. Optics* **38**, 599 (1999).
- 6) B. Labani, J. Bonamy, D. Robert, J. M. Hartmann, and J. Taine, *J. Chem. Phys.* **84**, 4256 (1986).
- 7) R. Lynch, R. R. Gamache, and S. P. Neshyba, *J. Chem. Phys.* **105**, 5711 (1996).
- 8) R. L. Cook and F. C. De Lucia, *Amer. J. Phys.* **39**, 1433 (1971).
- 9) G. W. King, R. M. Hainer, and P. C. Cross, *J. Chem. Phys.* **11**, 27 (1943).
- 10) L. S. Rothman, R. R. Gamache, R. H. Tipping, C. P. Rinsland, M. A. H. Smith, D. Chris Benner, V. Malathy Devi, J. -M. Flaud, C. Camy-Peyret, A. Perrin, A. Goldman, S. T. Massie, L. R. Brown, and R. A. Toth, *J. Quant. Spectrosc. Radiat. Transfer* **48**, 469 (1992).
- 11) R. O. Watts, *Chem. Phys.* **26**, 367 (1977).
- 12) M. Oobatake and T. Ooi, *Prog. Theor. Phys.* **48**, 2132 (1972).
- 13) *Numerical Recipes in Fortran 77*, edited by W. H. Press, S. A. Teukolsky, W. T. Vetterling, and B. P. Flannery A. Deepak, T. D. Wilkerson, and L. H. Runke, Cambridge University Press, (1992).
- 14) D. E. Burch, *SPIE Proc.* **277**, 28 (1981); D. E. Burch and D. A. Gryvnak, Report No. AFGL-TR-79-0054, 1979; D. E. Burch and R. L. Alt, Report No. AFGL-TR-84-0128, 1984; D. E. Burch, Report No. AFGL-TR-85-0036, 1985.

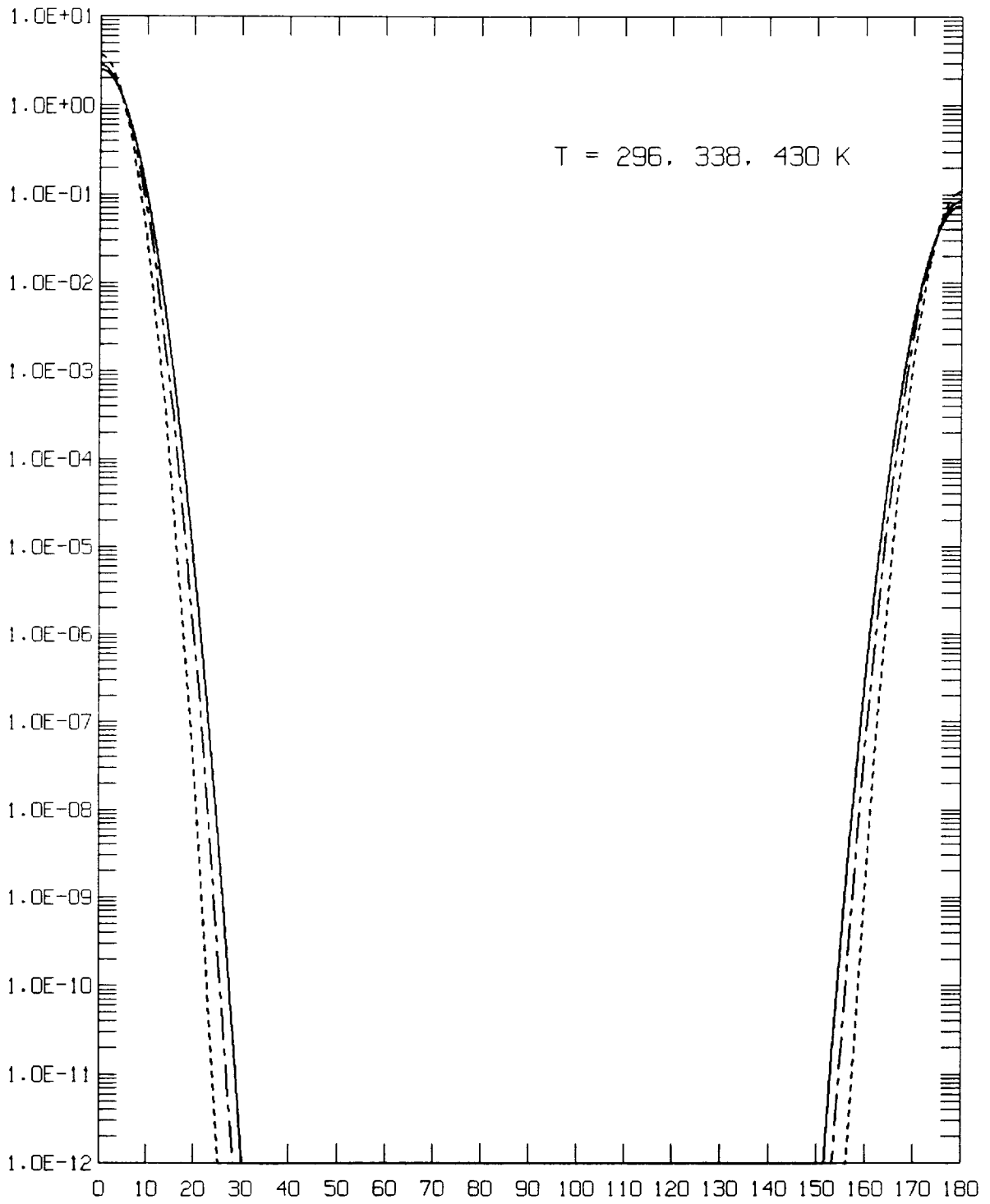
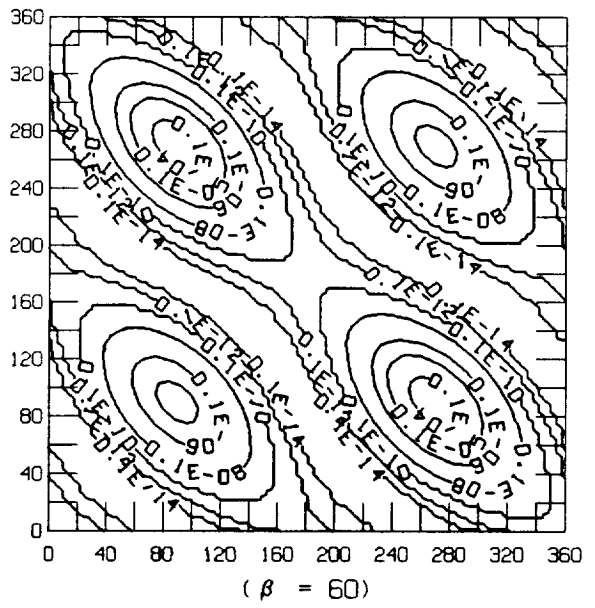
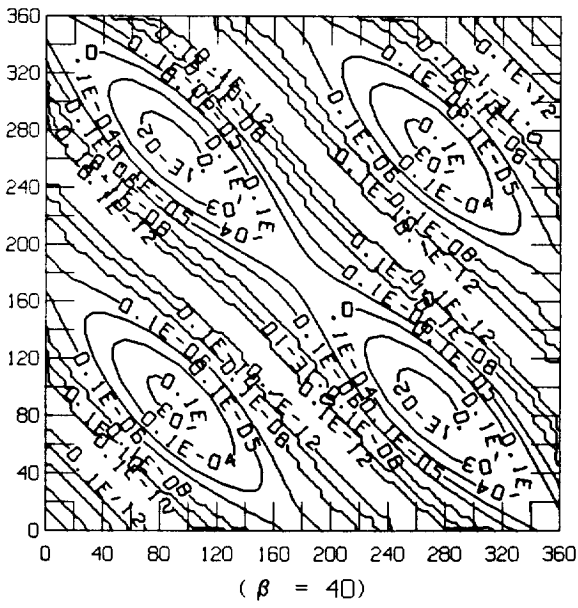
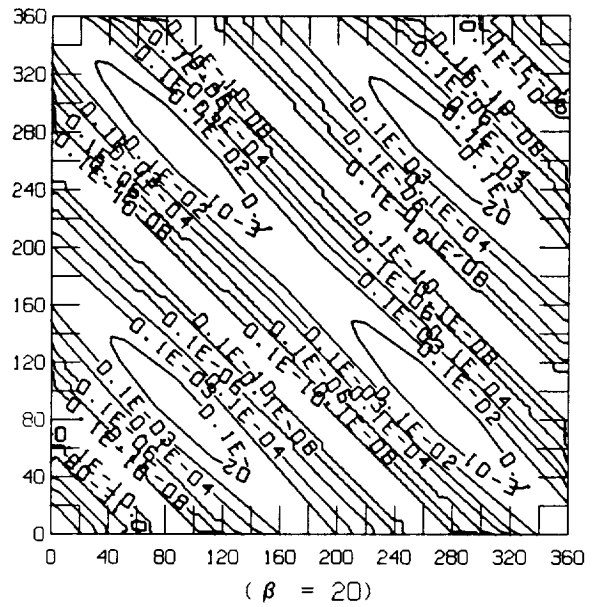
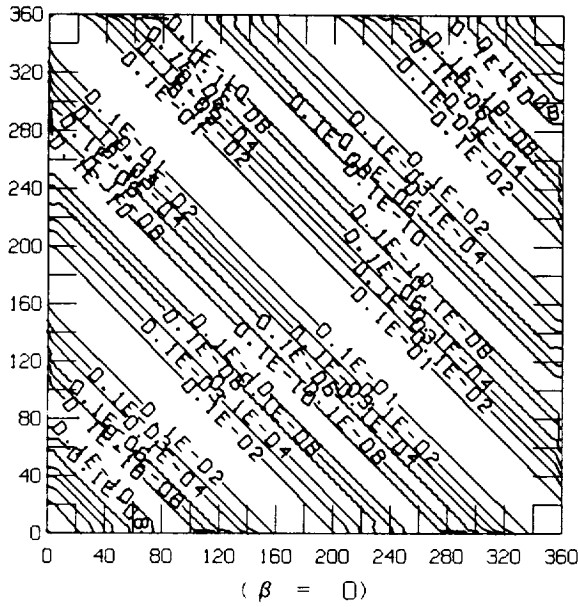
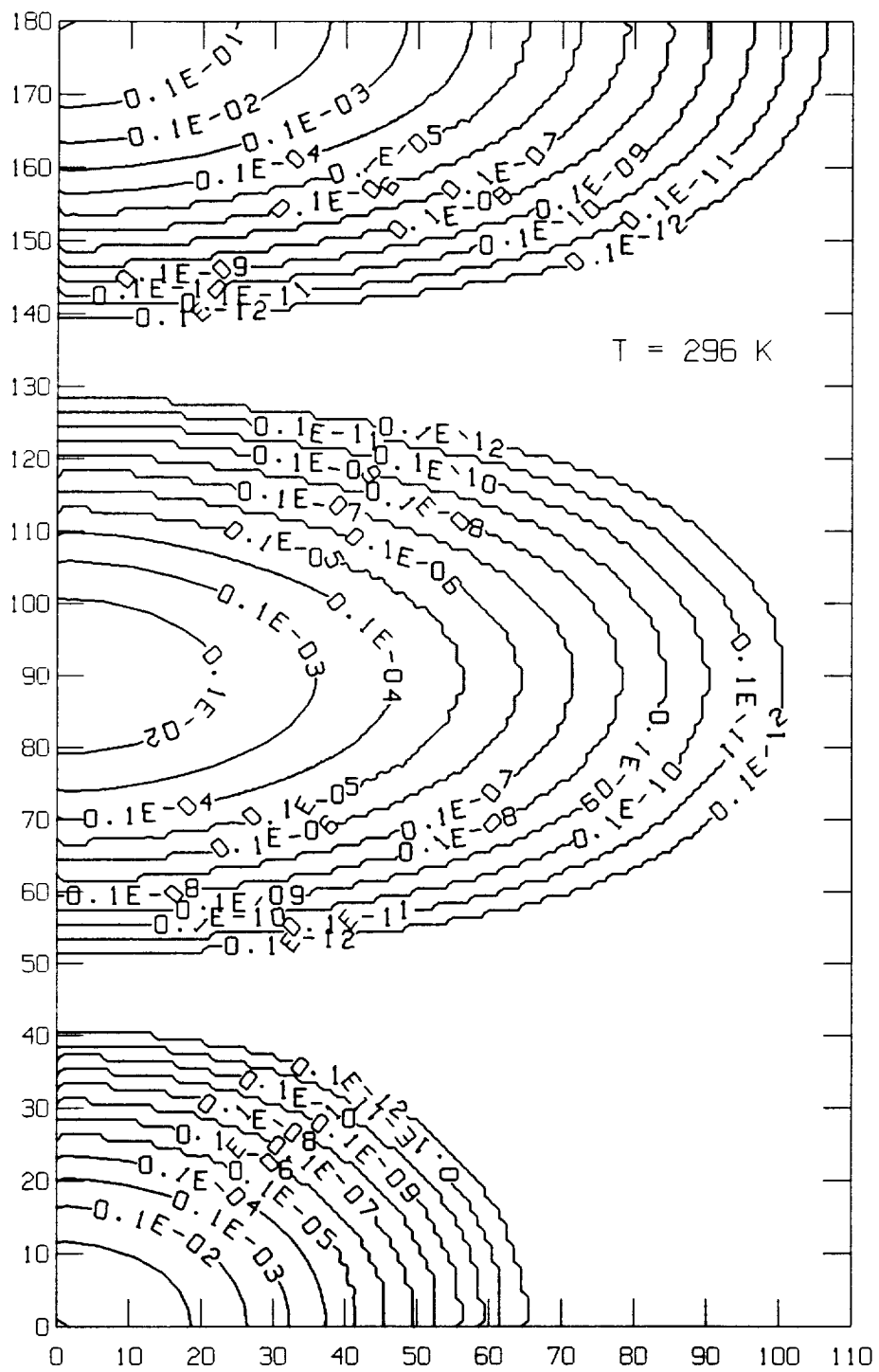
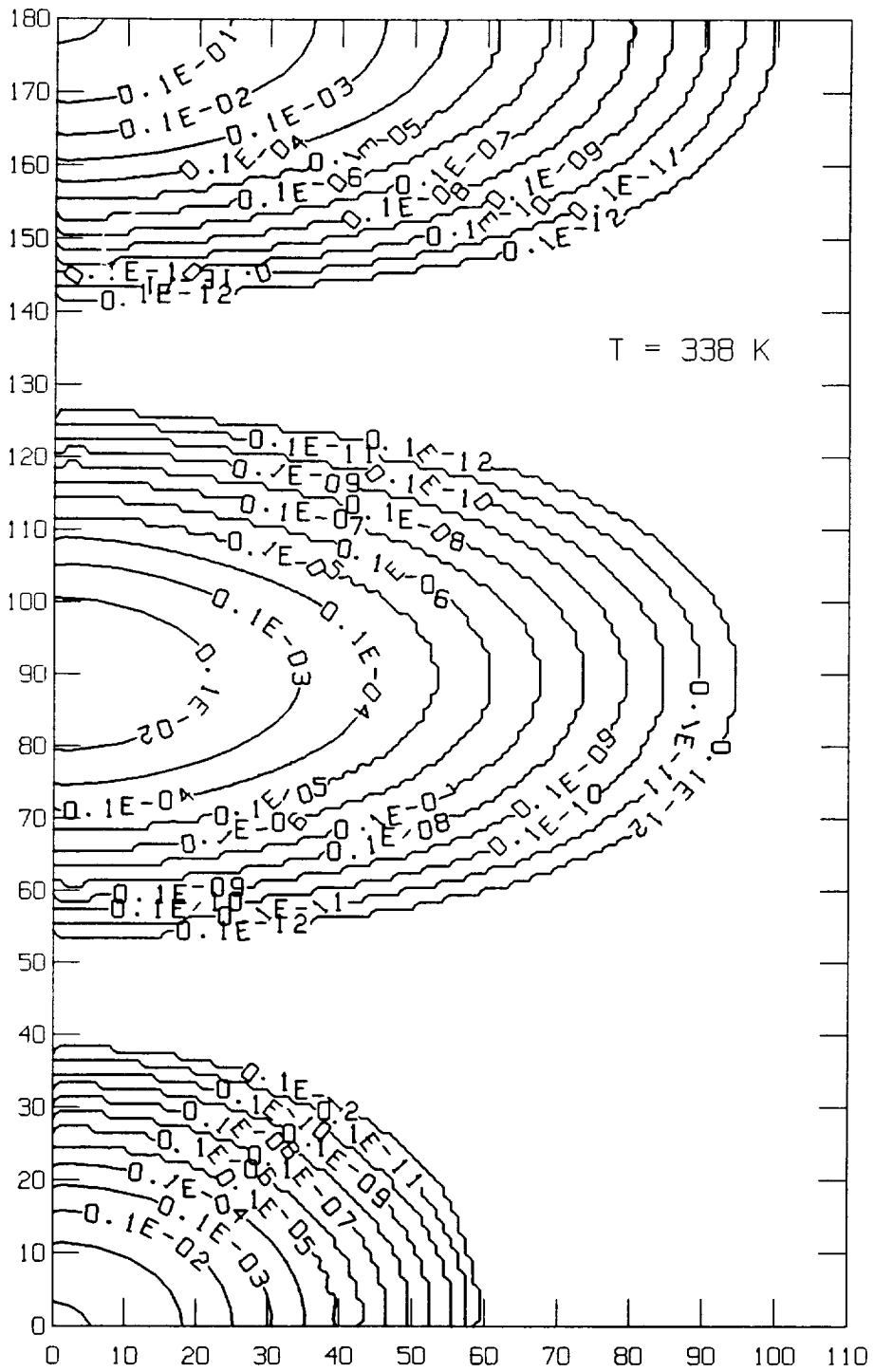


Fig. 1



T. 100





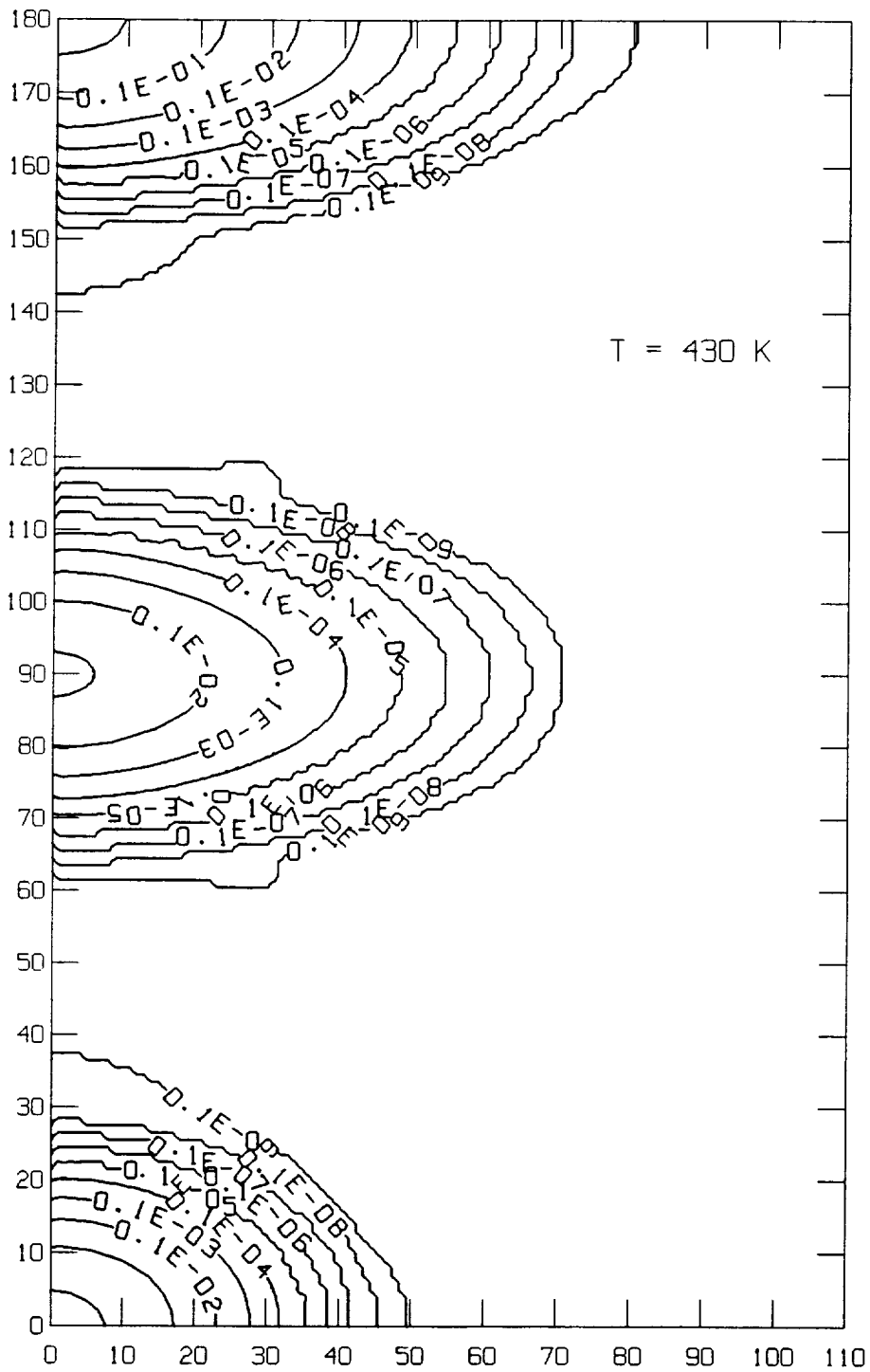
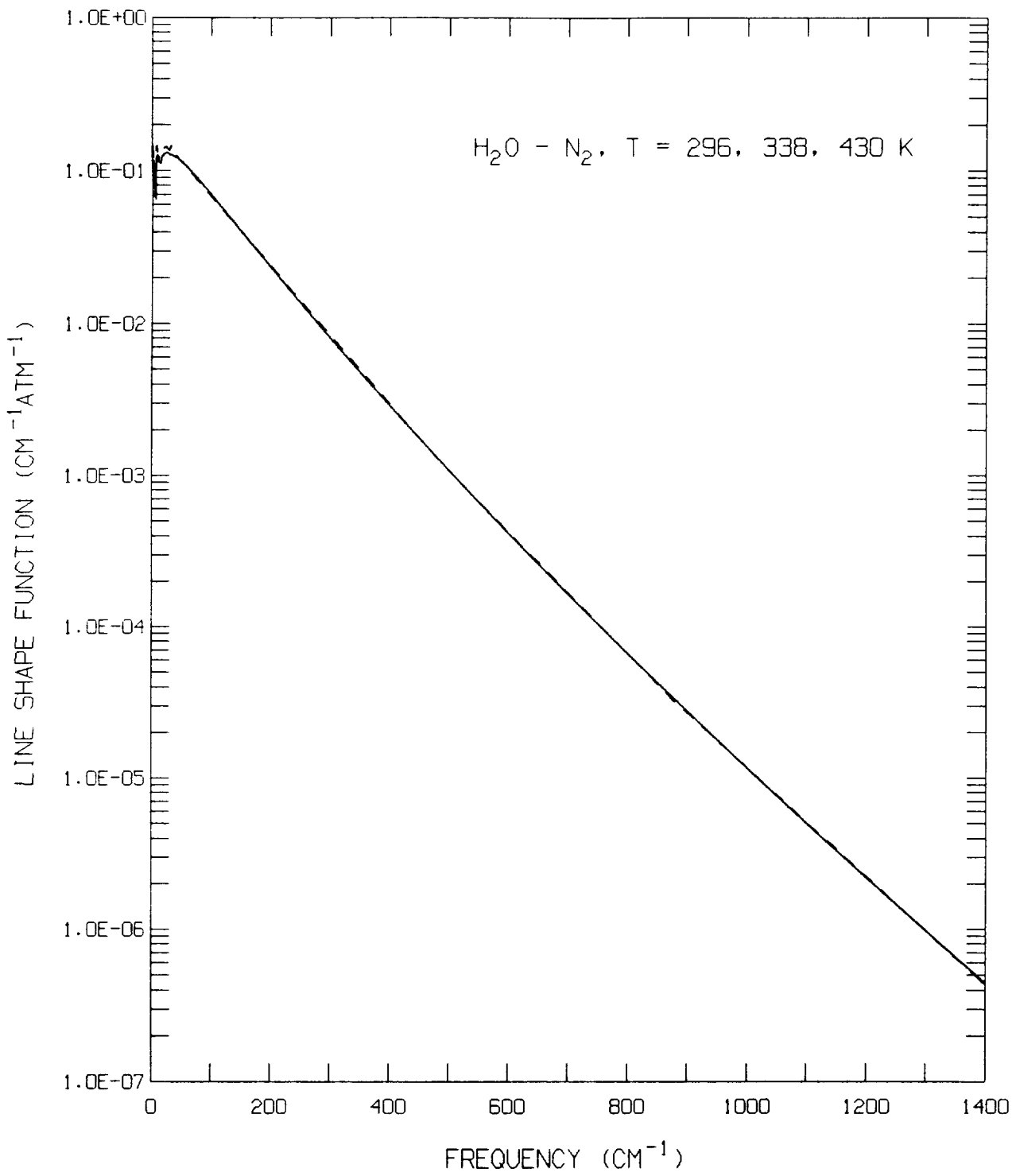
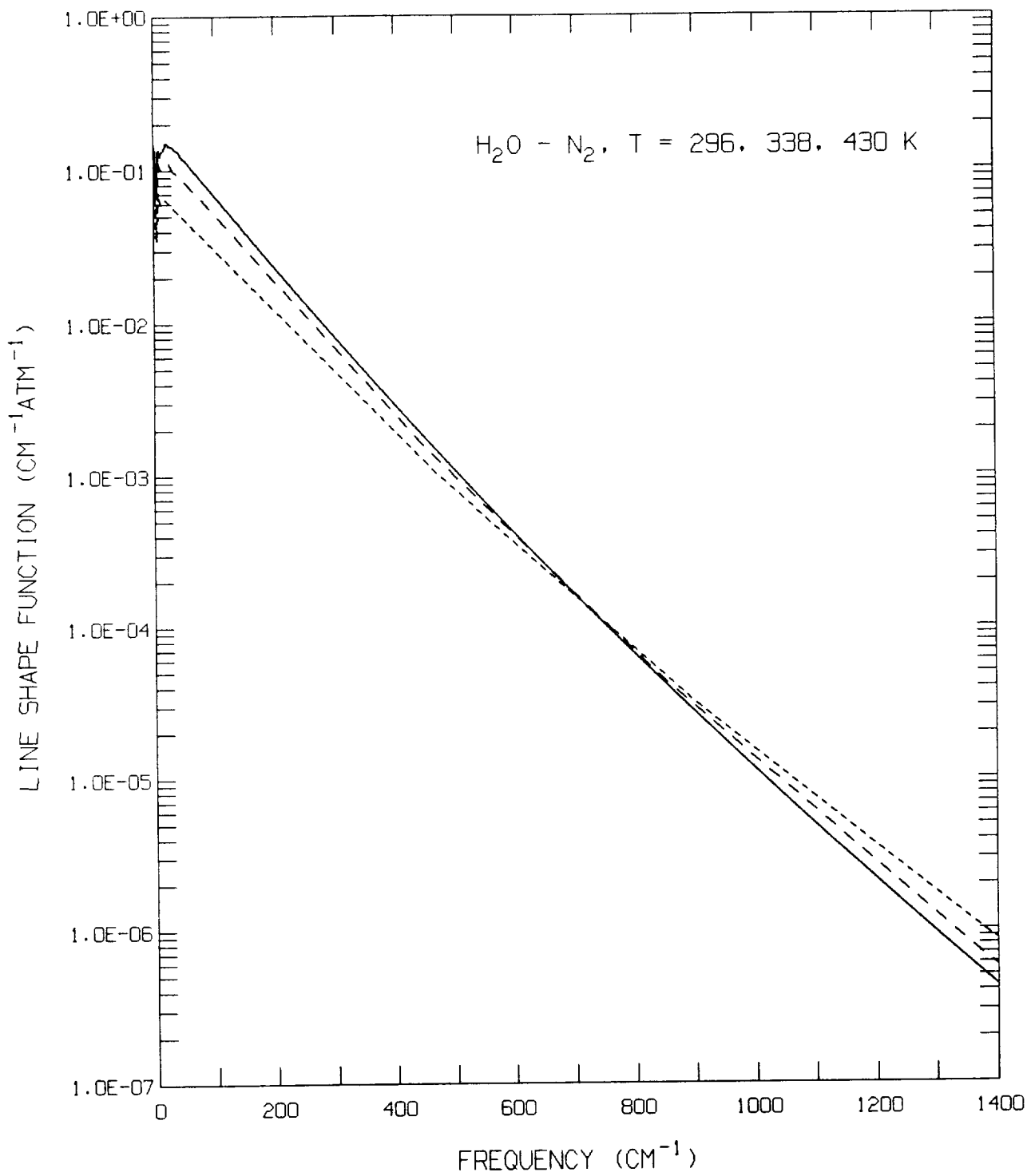


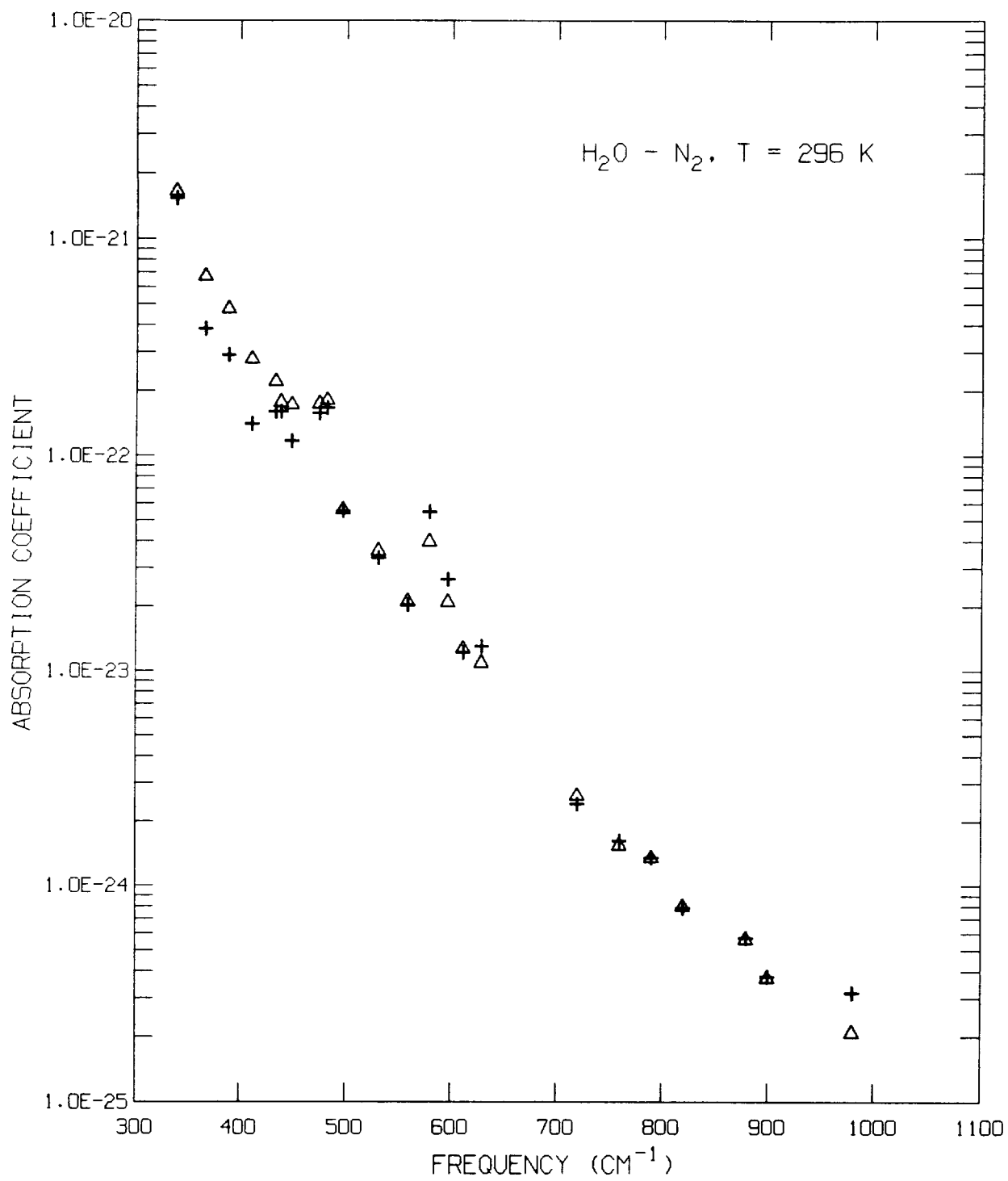
Fig 1



F 11



7.7



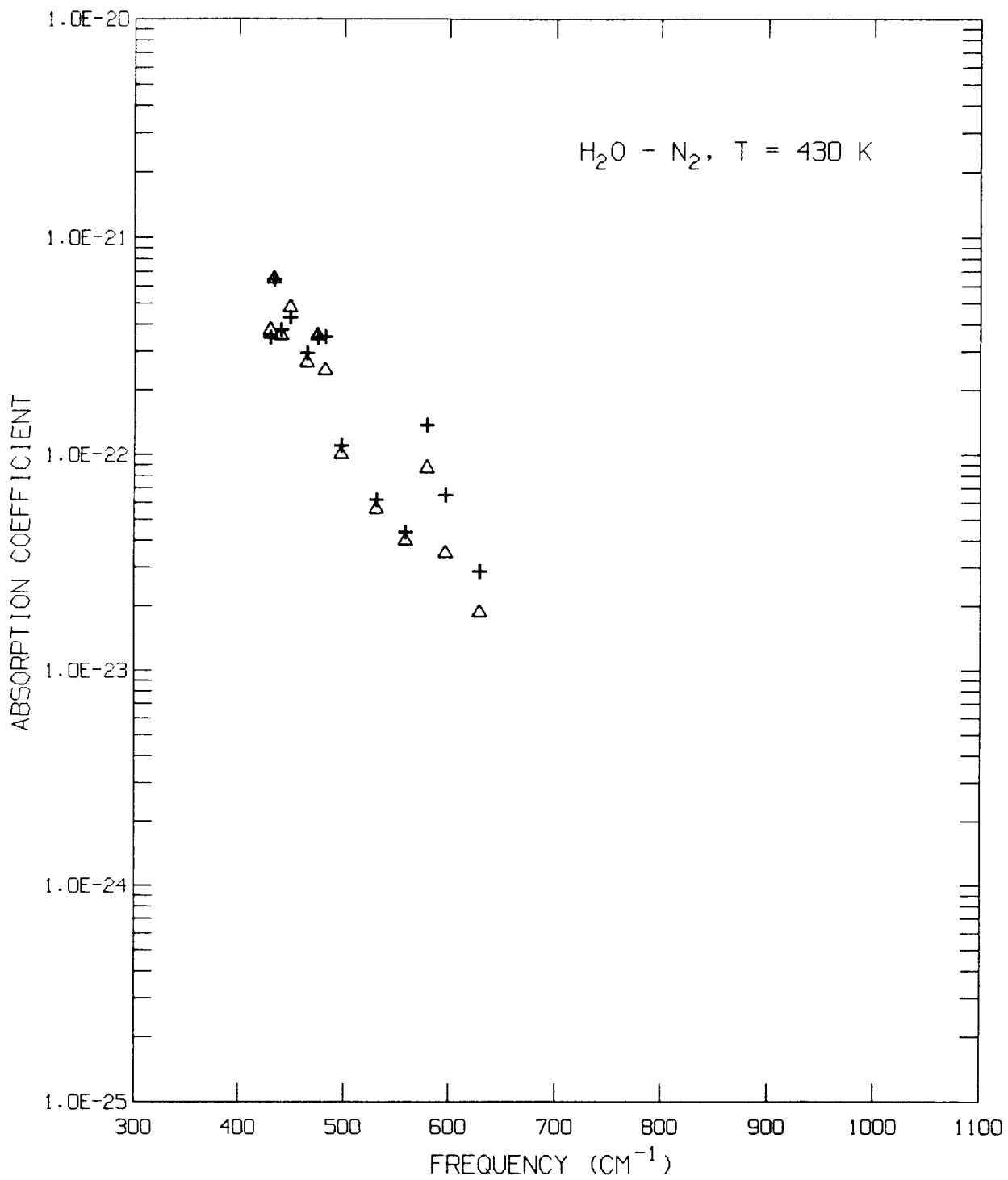


Fig. 9